Journal of Nanobiotechnology

RESEARCH

Open Access

Translational selenium nanomedicine synergizes with nab-paclitaxel to enhance antitumor effects in esophageal squamous cell cancer via selenoprotein N-mediated ER stress

Haoyang Huang[1], Shaowei Liu[1], Ligeng Xu[3], Hengrui Liang[1], Zihao Wu[3], Tianfeng Chen[3*], Jinlin Wang[2*] and Jun Liu[1*]

Abstract

Though prescribed as first-line drugs for esophageal squamous cell cancer (ESCC) therapy, the antitumor efficacy of Nab-Paclitaxel (Nab-PTX) is still unsatisfactory owing to the limitation on the dosage and therapy duration of Nab-PTX caused by adverse effects. Inspired by the very essential role of Selenoprotein N (SelN) in mediating the calcium homeostasis and the associated redox homeostasis in cells, herein, in this essay, we screened the inhibition effect of selenium-containing drugs in different forms on ESCC cell line. Investigation on KYSE-150 cells demonstrated that Nab-PTX in combination with low dosage of LNT-SeNPs may synergistically improve its antitumor efficacy on ESCC cells through promoting the cellular apoptosis. Proteomics analysis uncovered the core synergistic mechanism of LNT-SeNPs on Nab-PTX was significantly dependent on the endoplasmic reticulum (ER) stress induced by SelN-mediated Ca^{2+}-IRE1α, IRE1α(S724)-CHOP-BCL2 axis. SelN knockdown KYSE-150 cell model further confirmed the very indispensable role of SelN in mediating the synergistic effect on Nab-PTX. Moreover, in vivo evaluation on KYSE-150 tumor-bearing mice models also demonstrated the supplementation of LNT-SeNPs with low dosage during the Nab-PTX treatment may synergize the antitumor efficacy and significantly mitigate the adverse reactions or toxicity resulting from a substantial dose of Nab-PTX. Overall, along with the facile accessibility of raw materials, this study reports LNT-SeNPs as a synergistic agent to promote the antitumor efficacy of Nab-PTX, which may be translated as a wide-applicable, efficient and highly safe strategy for clinical treatment of ESCC.

*Correspondence:
Tianfeng Chen
tchentf@jnu.edu.cn
Jinlin Wang
wangjinlin@gird.cn
Jun Liu
ljxwkgy@126.com

Full list of author information is available at the end of the article

Graphical abstract

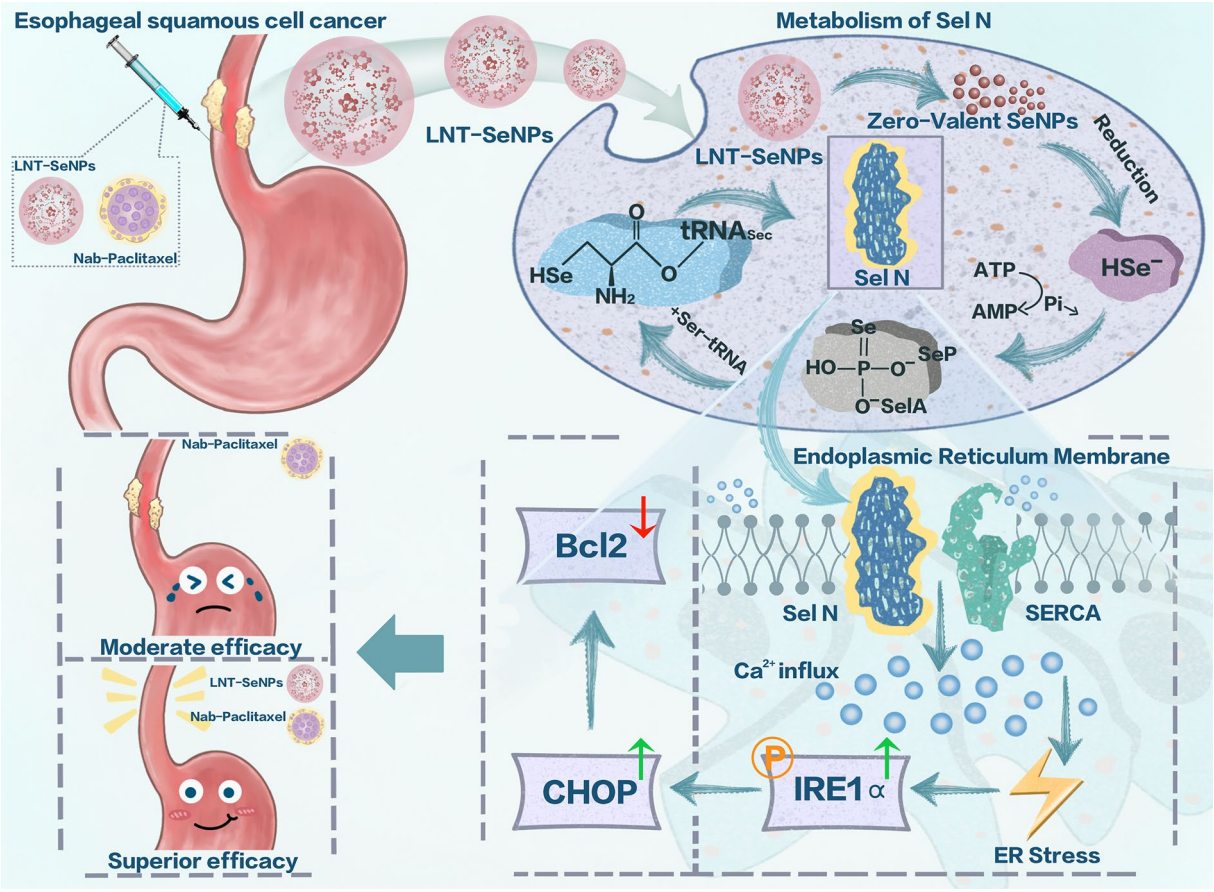

Keywords Selenium nanoparticles, Selenoprotein, Esophageal squamous cell cancer, ER stress

Introduction

Esophageal squamous cell cancer (ESCC), as a highly aggressive malignancy tumor, generally has two primary types with squamous cell carcinoma accounted as more prevailed type, which accounted for enormous mortality worldwide [1–4]. Currently, the prevailing treatment modalities for ESCC are focused on surgery, radiation therapy, chemotherapy etc. depending on the stage of the cancer [5]. For most locally advanced ESCC, a combination modality of chemotherapy and radiation therapy (known as neoadjuvant therapy) is primary strategy to be employed, especially for those patients who are not suitable for surgery [6–8]. Nab-Paclitaxel (Nab-PTX) representing as an innovative formulation of the conventional paclitaxel, has been exploited both as a monotreatment candidate or a combinative therapy with other chemotherapeutic drugs such as carboplatin, and 5-FU for advanced, unresectable, or metastatic ESCC [9–11]. While it offers some advantages over traditional paclitaxel, such as improved solubility and a potentially lower incidence of hypersensitivity reactions, adverse effects like neutropenia, peripheral neuropathy, nausea and diarrhea still limit the dosage and duration of Nab-PTX therapy [12]. Therefore, it's of great significance and urgency to exploit a wide-applicable, efficient and highly safe strategy to synergize the antitumor efficacy of Nab-PTX for ESCC [13]. Selenium (Se) as a trace element for maintenance of human health, exhibits an indispensable role in various physiological processes, e.g. cellular redox homeostasis, thyroid hormone metabolism, and immune function [14–18]. Over the years, Accumulating evidence has highlighted the potential antitumor effects of selenium, with observational studies suggesting an association between higher selenium levels (from diet or supplements) and a reduced risk of certain cancers, such as prostate, lung, and colorectal cancers, although the optimal levels for cancer prevention remain to be fully determined [19–23]. Generally, the physiological function of selenium element is mediated through its role as a constituent of selenoproteins [24]. For now, 25

selenoproteins including the glutathione peroxidases, thioredoxin reductases, and thyroid hormone deiodinases etc. have been identified in the human genome [25–31]. Among them, selenoprotein N (SelN), a specific selenoprotein residing in the ER has garnered significant interest for cancer treatment due to its critical function in maintaining calcium balance and related redox stability [32]. In the recent investigation by Ester Zitoa et al., SelN was further demonstrated as a mediator to enhance its redox-dependent interaction with sarcoplasmic/endoplasmic reticulum (ER) calcium ATPase (SERCA) to replenish the calcium reservoir in ER [32]. Therefore, based on the antitumor mechanism of Nab-PTX, we're wondering whether it's feasible that the combinative therapy of Nab-PTX (the first-line drug for ESCC) and selenium may improve the treatment outcome of ESCC. However, high dosage of small-molecule selenocompounds supplementation (e.g. selenite) can be toxic, leading to selenosis, a condition with symptoms including gastrointestinal distress, hair loss, nail changes. In more severe cases, neurological damage was also reported [33]. The narrow margin between beneficial and toxic doses thus confines the wide application of selenium as a therapeutic agent [33]. Compare with small-molecule selenocompounds, Se nanoparticles (SeNPs) with great biocompatibility, delicate size effect and interfacial properties has approved its great potency in treating various diseases such as cancer, influenza, osteoporosis, and allergic dermatitis [34–44]. Therefore, in this essay, we screened the inhibition effect of selenocysteine ($SeCys_2$), selenomethionine (SeMet), sodium selenite (Na_2SeO_3), and translational selenium nanoparticles coated with lentinan (LNT-SeNPs) on ESCC cell line (KYSE-150 cells) and revealed the underlying synergistic potential of LNT-SeNPs on promoting the antitumor efficacy of Nab-PTX. Investigation on KYSE-150 cells demonstrated that Nab-PTX in combination with low dosage (8 μM) of LNT-SeNPs may synergistically improve its antitumor efficacy on ESCC cells through promoting the apoptosis and inhibiting the metastasis. Proteomics analysis revealed the core mechanism of LNT-SeNPs (Scheme 1) on promoting the antitumor efficacy of Nab-PTX

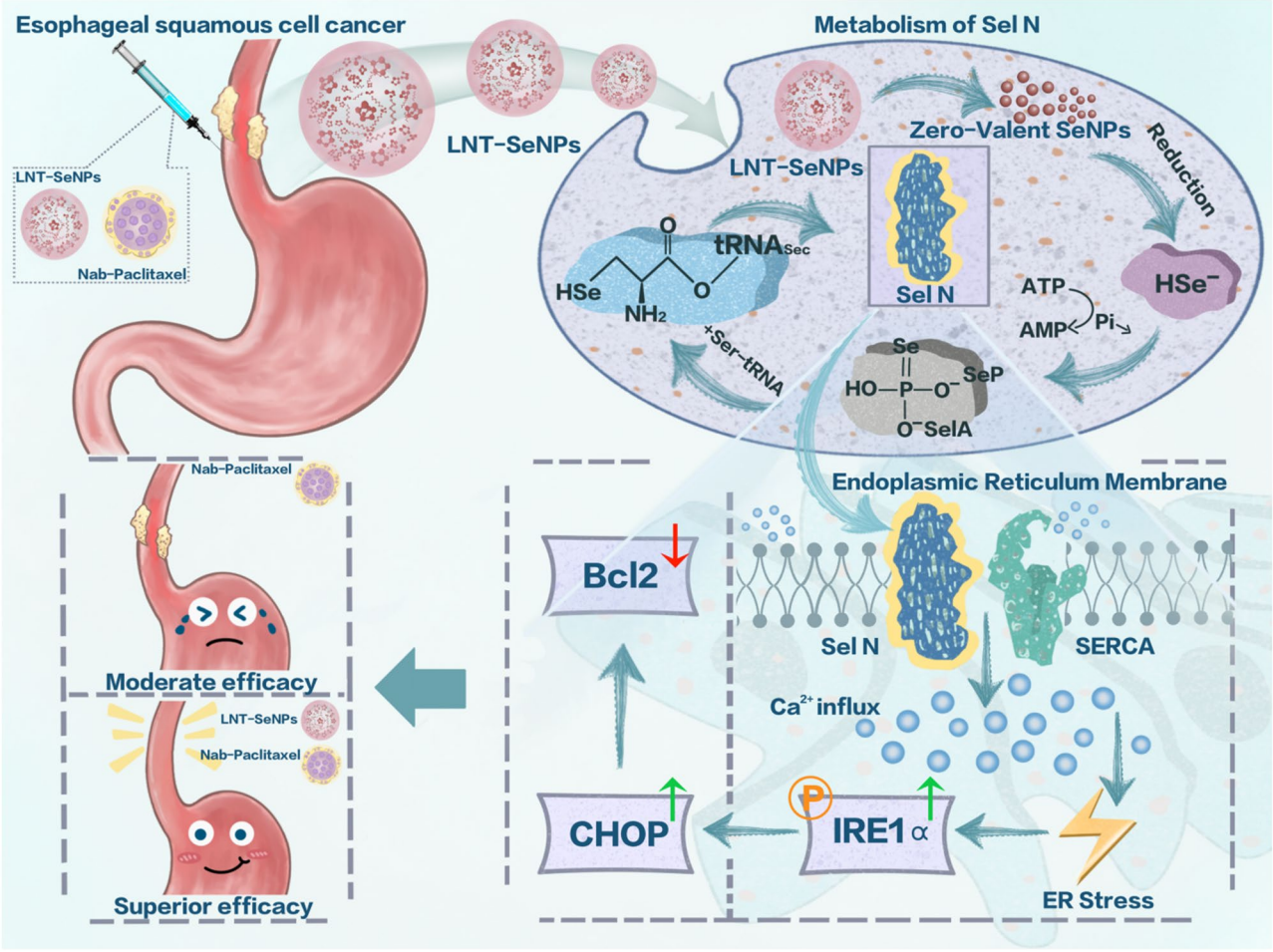

Scheme 1 Schematic illustration on the synergistic antitumor mechanism of LNT-SeNPs with Nab-Paclitaxel on esophageal squamous cell cancer through SelN-mediated Ca^{2+}-IRE1α(S724)-CHOP-BCL2 axis

was significantly relied on the excessive Ca^{2+} accumulation in ER induced by SelN-mediated Ca^{2+}-IRE1α, IRE1α (S724)-CHOP-BCL2 axis. SelN knockdown KYSE-150 cell model (KYSE-150/shSelN cells) further confirmed the very indispensable role of SelN in mediating the synergistic effect on promoting the antitumor efficacy of Nab-PTX. Moreover, in vivo evaluation of KYSE-150 tumor-bearing mice models also demonstrated the intravenous injection of LNT-SeNPs with low dosage during Nab-PTX therapy may synergize its antitumor efficacy and significantly alleviate the side-effects or toxicity. Overall, this essay reported LNT-SeNPs as a synergistic agent to promote the antitumor efficacy of Nab-PTX, which may be translated as a wide-applicable, efficient and highly safe strategy for clinical treatment of ESCC.

Results and discussion

Synergistic antitumor potential between LNT-SeNPs and Nab-PTX on ESCC

LNT-SeNPs were firstly prepared *via* the reaction between Na_2SeO_3 and Vitamin C (Vc). As observed in Fig. 1A, the as-prepared LNT-SeNPs exhibited in spherical shape with an average size of 100 nm, suggesting the successful preparation. The diameter increasement (~126.8 nm) and the negatively charged surface (Fig. 1B) further demonstrated the coating of LNT. The structure of LNT-SeNPs was then studied by XPS. As indicated in Fig. 1C, Se 3d at 53.48 eV was detected in the XPS spectrum of LNT-SeNPs, demonstrating the successful preparation. The data of UV spectrometer (Figure S1) further confirmed the structure of LNT-SeNPs as a similar absorbance curve could be detected between SeNPs and LNT-SeNPs. Taken together, all these data demonstrated the successful preparation of monodispersed LNT-SeNPs.

According to our previous researches about the antitumor mechanism of SeNPs on various cancer types, SeNPs may synergize the antitumor efficacy of different chemotherapeutics through selenoprotein-mediated signaling pathways. Therefore, we're wondering whether it's feasible that the combinative therapy of Nab-PTX (the first-line drug for ESCC) and SeNPs may improve the treatment outcome of ESCC. Therefore, the cytotoxicity of different selenium-containing drugs ($SeCys_2$, SeM, Na_2SeO_3, and LNT-SeNPs) was firstly screened on KYSE-150 cells. As indicated in Fig. 1D, all these drugs exhibited inhibition effect on the proliferation of KYSE-150 cells in different extents. However, it should be noted that Na_2SeO_3 exhibited much stronger cytotoxicity than the other drugs owing to its selenite free form. Besides that, in comparison with the low inhibition effect of SeM in a relatively wide concentration range and the toxicity potential of $SeCys_2$ in relatively high concentration (>8 μM), LNT-SeNPs were thus chosen as the selenium-containing drugs for the following investigations. Meanwhile, it was demonstrated that Nab-PTX exhibited apparent antitumor activity when its concentration larger than 32 ng/mL (Fig. 1E). After that, the combination antitumor effect between LNT-SeNPs and Nab-PTX on KYSE-150 cells was further investigated. As shown in Fig. 1F and I, the antitumor efficacy of Nab-PTX was significantly improved under the influence of LNT-SeNPs in a dose-dependent manner (1–8 μM). Besides that, it's noteworthy that, although LNT-SeNPs amplify the antitumor efficacy of Nab-PTX, its monotreatment with KYSE-150 cells all exhibited low cytotoxicity with cell viability high up to ~90%. Therefore, the synergistic effect between LNT-SeNPs and Nab-PTX was analyzed by SynergyFinder software. It could be seen in Fig. 1J, the ZIP synergy score of these two drugs was 17.809, indicating a strong synergistic effect. Concluding from all these results, it could be deduced that LNT-SeNPs may significantly synergize the antitumor efficacy of Nab-PTX on ESCC while still preserving low toxicity to cells, which is highly feasible to be applied in the ESCC treatment.

LNT-SeNPs synergize the antitumor efficacy of Nab-PTX at low dosage

Inspired by the above results, the antitumor mechanism of LNT-SeNPs and Nab-PTX was further investigated. As shown in Fig. 2A, in comparison with the strong red fluorescence in control group, the monotreatment of LNT-SeNPs or Nab-PTX partially inhibited the cell proliferation as only scattered red fluorescence spot could be observed under microscope. While in the Compound group, red fluorescence was hardly to be detected, demonstrating the great antitumor efficacy of LNT-SeNPs and Nab-PTX. The physiological effect of nanoparticles was always accompanied with its highly efficient cellular uptake. Therefore, whether the co-treatment with Nab-PTX would influence the cellular uptake of LNT-SeNPs intrigued us. The cellular uptake of LNT-SeNPs by KYSE-150 cells was thus verified. As shown in Fig. 2B and Figure S2-S3, both LNT-SeNPs group and Compound group exhibited very efficient uptake and similar uptake trends of LNT-SeNPs, confirming the feasibility of co-treatment of LNT-SeNPs and Nab-PTX.

The antitumor mechanism of LNT-SeNPs and Nab-PTX co-treatment was thus investigated by flow cytometry. As show in Fig. 2C, in comparison with control group, the monotreatment of Nab-PTX significantly enhanced the cell cycle arrest at subG1 phase to 8.25% while the LNT-SeNPs did not influence the cell cycle of KYSE-150 cells as the cell cycle distribution was comparable to the control group. Intriguingly, in Compound group, the cell cycle arrest at subG1 phase was further elevated for 25% in comparison with Nab-PTX group, verifying the synergistic effect between LNT-SeNPs and Nab-PTX. At the same time, both Nab-PTX and Compound

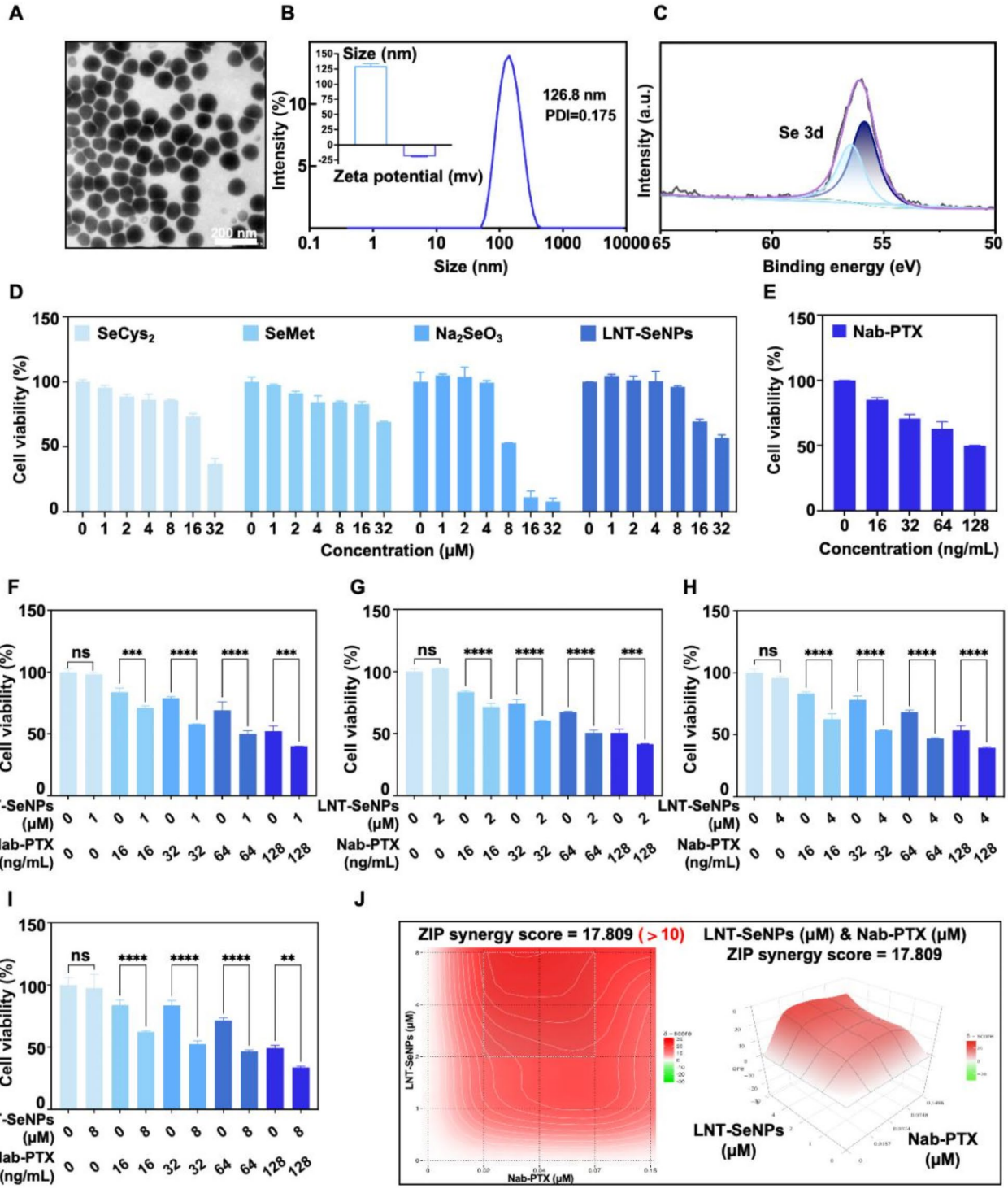

Fig. 1 Preparation of LNT-SeNPs and its synergistic antitumor potential with Nab-PTX on KYSE-150 cells. (**A**) Morphology of LNT-SeNPs characterized by TEM. (**B**) Hydrodynamic size distribution and zeta potential of LNT-SeNPs analyzed by Malvern Zetasizer. (**C**) The binding energy of Se 3d in LNT-SeNPs. (**D**) Cell viability of KYSE-150 cells treated with serials concentration (0–32 μM) of various selenium-containing drugs ($SeCys_2$, SeMet, Na_2SeO_3, LNT-SeNPs) after 48 h. (**E**) Cell viability of KYSE-150 cells treated with serial concentrations (0-128 ng/mL) of Nab-PTX after 48 h. (**F**-**I**) Cell viability of KYSE-150 cells co-treated with Nab-PTX (0-128 ng/mL) and LNT-SeNPs (1–8 μM) after 48 h. (**J**) Synergistic antitumor effect between LNT-SeNPs and Nab-PTX analyzed by SynergyFinder with a ZIP synergy score of 17.809 (synergy score > 10 indicates synergistic sensitization). All data are shown as mean ± SD ($n = 3$). *$P < 0.05$, **$P < 0.01$, ***$P < 0.001$, ****$P < 0.0001$

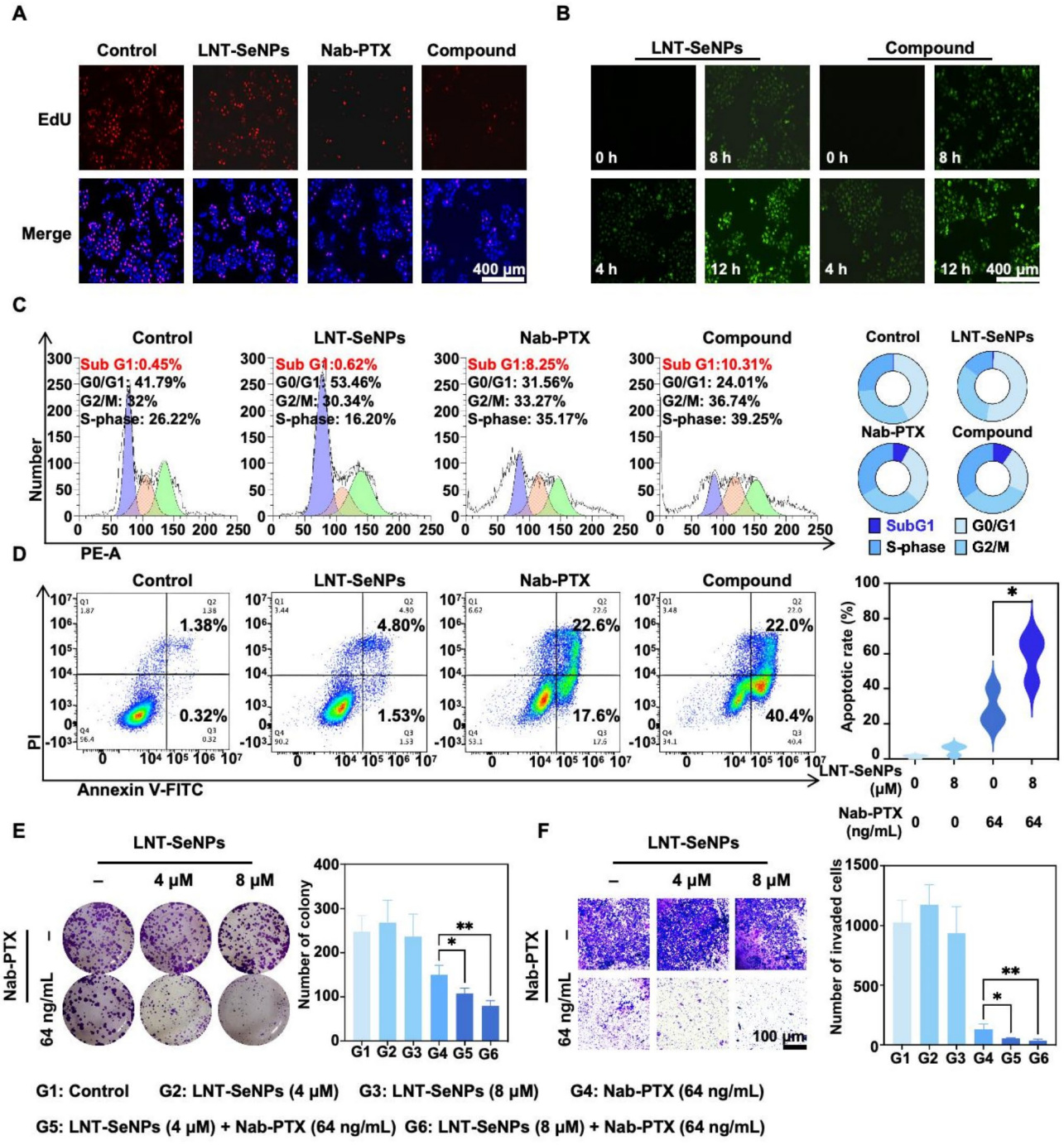

Fig. 2 LNT-SeNPs synergize the antitumor efficacy of Nab-PTX on KYSE-150 cells at low dosage. (**A**) The antitumor efficacy of LNT-SeNPs and Nab-PTX on KYSE-150 cells detected by EdU assay kits. (**B**) Representative fluorescent images of cellular uptake of KYSE-150 cells cultured with coumarin-**6**-loaded LNT-SeNPs or the Compound (coumarin-**6**-loaded LNT-SeNPs + Nab-PTX) for 12 h. (**C**) Cell cycle distribution and quantitative analysis of KYSE-150 cells after treated with LNT-SeNPs and Nab-PTX for 48 h. (**D**) Apoptosis of KYSE-150 cells (Annexin V-FITC/PI staining) induced by LNT-SeNPs and Nab-PTX. (**E**) Representative photos of colony formation of KYSE-150 cells treated with LNT-SeNPs and Nab-PTX for 14 days. (**F**) Representative photos of transwell invasion assay of KYSE-150 cells treated with LNT-SeNPs and Nab-PTX for 24 h. All data are shown as mean ± SD ($n = 3$). *$P < 0.05$, **$P < 0.01$, ***$P < 0.001$, ****$P < 0.0001$

groups especially the latter one significantly induced S phase arrest up to about 40%, in comparison with control group. The analysis on the apoptotic cells (Fig. 2D) by flow cytometry further confirmed its synergistic effect on KYSE-150 cells as the apoptotic ratio in Compound group (62.4%) was 55.2% higher than that from Nab-PTX group (40.2%). After demonstrating the strong synergistic effect of LNT-SeNPs and Nab-PTX on inducing cells apoptosis. Its antitumor efficacy was further investigated by colony formation assay. As indicated in Fig. 2E, the monotreatment of LNT-SeNPs did not exhibit inhibition effect on the colony formation of KYSE-150 cells, even promote the colony formation under 4 μM. In contrast, after combination with Nab-PTX, the colony formation of KYSE-150 cells was significantly decreased even compared with Nab-PTX group. Metastasis is commonly reported at the later stage of ESCC. Therefore, the in vitro invasion assay was conducted to evaluate the anti-metastatic efficacy of LNT-SeNPs and Nab-PTX co-treatment. As shown in Fig. 2F, the co-treatment of LNT-SeNPs and Nab-PTX significantly decreased the invaded cells from ~1000 to only ~33, indicating the effect of LNT-SeNPs and Nab-PTX co-treatment on inhibiting the ESCC metastasis.

Taken together, all these data demonstrated that Nab-PTX in combination with low dosage (8 μM) of LNT-SeNPs may synergistically improve its antitumor efficacy on ESCC cells through promoting the apoptosis and inhibiting the metastasis.

LNT-SeNPs synergize the antitumor efficacy of Nab-PTX through selenoprotein-mediated ER stress

After demonstrating the synergistic effect between LNT-SeNPs and Nab-PTX on ESCC, its underlying mechanism was further investigated by proteomics analysis. As indicated in Fig. 3A, protein expressions between control group and LNT-SeNPs group or Compound group exhibited significant differences, and the differentially expressed proteins were further identified as illustrated in Fig. 3B. To date, selenium nanoparticles including LNT-SeNPs generally fulfill its antitumor efficacy or other physiological functions through selenoprotein as outlined in Fig. 3C. Therefore, the selenoprotein expression in KYSE-150 cells/SelN knockdown KYSE-150 cells treated with LNT-SeNPs and Nab-PTX was analyzed by proteomics. As shown in Fig. 3D, compared with the control group, both the LNT-SeNPs group and Compound group significantly elevated the selenoprotein-related expression including SELENOH, SELENON, SEPHS2, TXNRD1, TXNRD2, and GPX4 in different extents. It should be noted that the expression of SELENON (SelN) was the highest, which was ~2 fold to the control group, indicating the influence of SelN on mediating the signaling pathways. Therefore, the SelN expression stimulated by LNT-SeNPs was further confirmed by western blotting analysis. As shown in Fig. 3E, compared with Control groups, in both the LNT-SeNPs and Compound groups, the expression of SelN in KYSE-150 cells was upregulated by 1.2-fold due to the action of LNT-SeNPs. However, in SelN knockdown KYSE-150 cells (KYSE-150/shSelN), LNT-SeNPs did not induce a significant upregulation of SelN, indicating that the upregulation of SelN in KYSE-150 cells is dependent on the induction by LNT-SeNPs. Moreover, in SelN knockdown KYSE-150 cells treated with Compound group, though under the stimulation of Nab-PTX, the expression of SelN was still comparable to control, highlighting the essential role of LNT-SeNPs in mediating the antitumor-related signaling pathways.

According to the relevant reports, SelN is a kind of selenoprotein to maintain the cellular redox homeostasis and redox-related calcium homeostasis through regulating the calcium pump ATP2A2 to protect ER against oxidative damage. Therefore, the correlation between calcium level and ER function was further investigated. As shown in Fig. 3F, strong green fluorescence could be detected in both LNT-SeNPs and Compound group. While in the Nab-PTX group, although the green fluorescence was detectable, the intensity was much weaker than that of the other two treatment groups. All these results collectively indicated that, the excessive Ca^{2+} accumulation in ER induced by LNT-SeNPs-mediated ER stress-related signaling pathways is the core mechanism to clarify its synergistic effect on promoting the antitumor efficacy of Nab-PTX on esophageal cancer. The enrichment analysis was thus further investigated to prove the above speculation. As shown in Fig. 3G and H, Gene Set Enrichment Analysis (GSEA) suggested that, compare with the control group, genes stimulated by LNT-SeNPs group or Compound group both enriched in protein processing in ER pathways, verifying the proposal of SelN-mediated ER stress. KEGG (Fig. 3I and J) and GO (Figure S5) enrichment analysis also demonstrated this speculation. Moreover, the protein-protein interaction network (PPI) analysis (Figure S6) highlighted the interactions between proteins influenced by LNT-SeNPs in KYSE-150 cells. Concluding from all these analyses, it could be demonstrated that the synergistic antitumor efficacy between LNT-SeNPs and Nab-PTX on ESCC was mainly relied on SelN-mediated ER stress.

The mechanism on SelN-mediated ER stress induced by LNT-SeNPs and Nab-PTX was then further investigated

As shown in Fig. 4A, ER stress-related differentially expressed genes including EIF2S1, SelN, WFS1, and MAP2K7 were firstly identified. The associated protein expressions were further verified by proteomics. As indicated in Fig. 4B, under the stimulation of LNT-SeNPs and Nab-PTX, ER stress-related proteins especially SSR4,

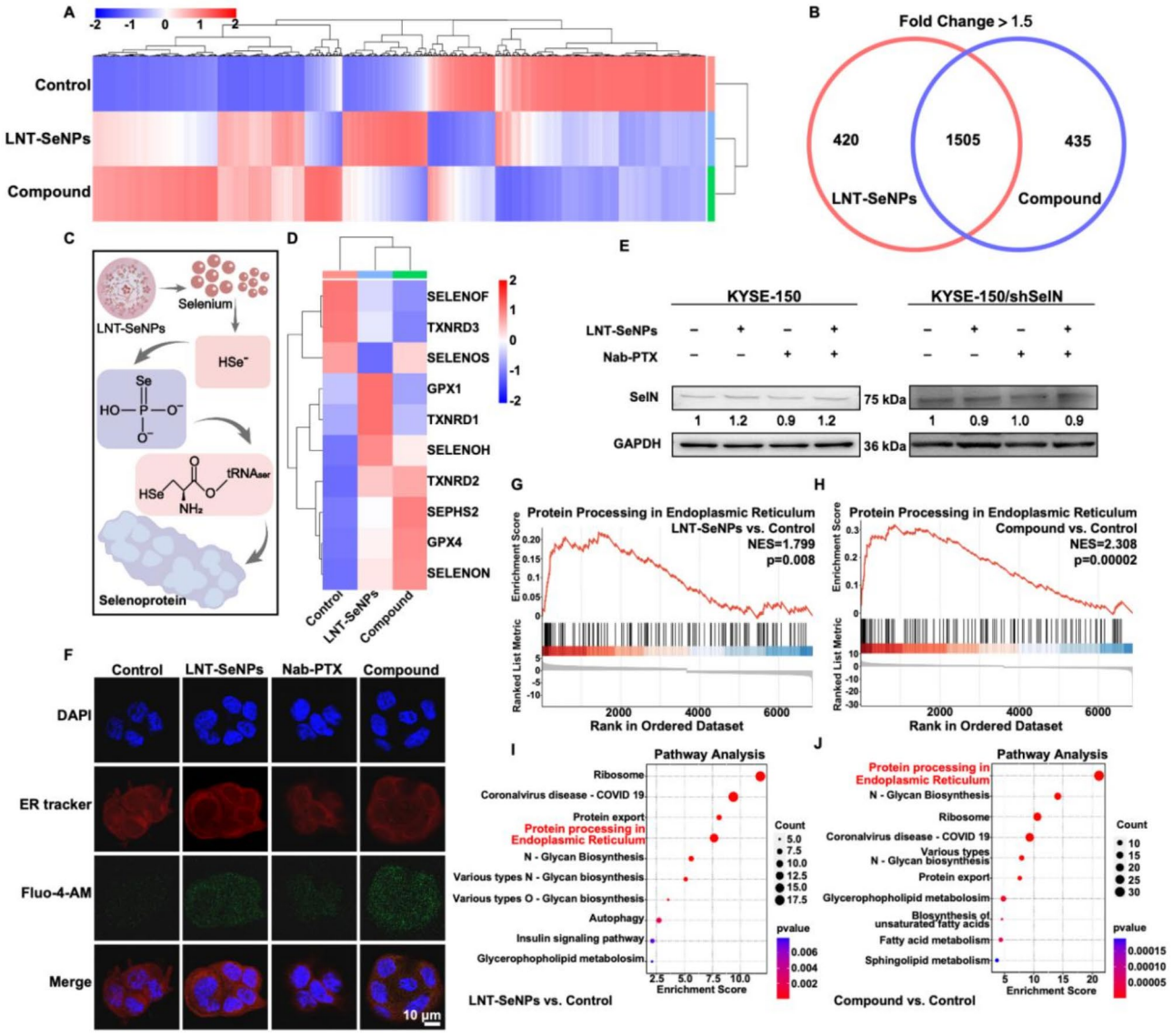

Fig. 3 Proteomics analysis of KYSE-150 cells treated with LNT-SeNPs and Nab-PTX. (**A**) Heat map of protein expression in KYSE-150 cells treated with LNT-SeNPs group (LNT-SeNPs) and LNT-SeNPs + Nab-PTX group (Compound). (**B**) Venn diagram depicting the distribution of differentially expressed proteins (Fold Change > 1.5) between the LNT-SeNPs and Compound groups, (**C**) The metabolic pathway of LNT-SeNPs from selenium into selenoproteins. (**D**) Heat map of selenoprotein expression in KYSE-150 cells treated with LNT-SeNPs group (LNT-SeNPs) and LNT-SeNPs + Nab-PTX group (Compound). (**E**) Expression of SelN in KYSE-150 cells treated with LNT-SeNPs, Nab-PTX, or both. (**F**) Representative images of ER tracker and Fluo-4-AM co-stained KYSE-150 cells after treated with LNT-SeNPs, Nab-PTX, or both, scale bar = 10 μm. GSEA enrichment analysis between the Control group and (**G**) LNT-SeNPs group or (**H**) the Compound group. KEGG enrichment analysis between the Control group and (**I**) LNT-SeNPs group or (**J**) the Compound group. All data are shown as mean ± SD ($n = 3$). *$P < 0.05$, **$P < 0.01$, ***$P < 0.001$, ****$P < 0.0001$

ERLEC1, MAP2K7 were greatly up-regulated, suggesting the activation of ER stress-related signaling pathways. The ER stress in KYSE-150 cells was thus visualized by TEM. As shown in Fig. 4C, normal ER in benign status (indicated by white arrow) could be observed in control group. While in LNT-SeNPs group, swollen ER was distinctively detected in the cytoplasm with red arrow pointed. This phenomenon could also be observed in the Compound group, with more autophagosomes detected in the cytoplasm compared with the Nab-PTX group, highlighting the very essential role of LNT-SeNPs in promoting the ER stress in KYSE-150 cells. Concluding from all these data and results, it could be speculated that (as illustrated in Fig. 4D), the up-regulation of SelN induced by LNT-SeNPs may interfere with the calcium pump, lead to the excessive Ca^{2+} accumulation in ER and finally result to the ER stress to facilitate the antitumor efficacy of Nab-PTX.

In order to confirm the indispensable role of SelN in mediating ER stress in KYSE-150 cells, SelN was knocked

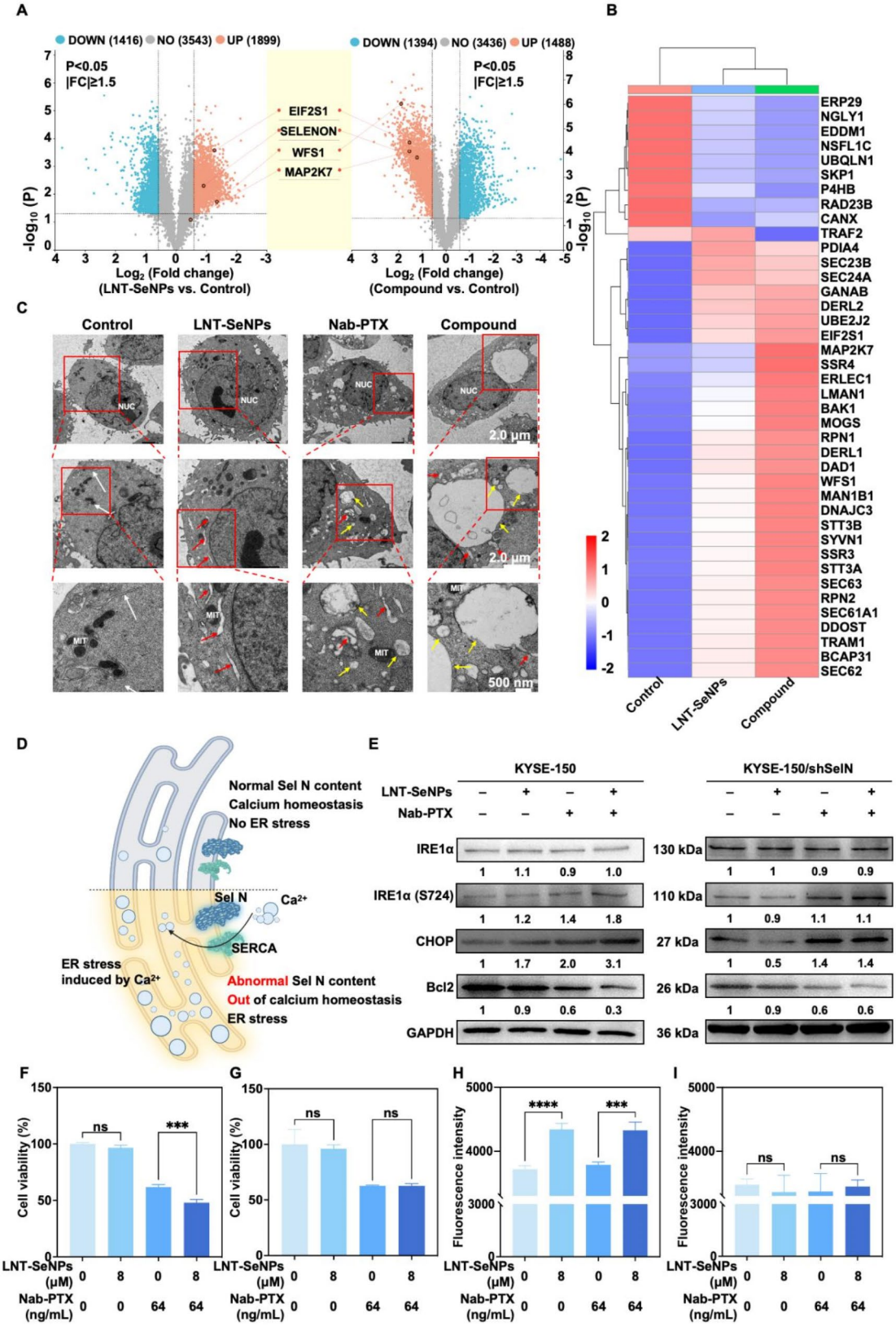

Fig. 4 (See legend on next page.)

(See figure on previous page.)

Fig. 4 Proteomics analysis on ER stress-related proteins. (**A**) Volcano plot of up- or down-regulated genes in KYSE-150 cells treated with the LNT-SeNPs and the Compound compare to the control group. (**B**) Heat map of ER stress-related proteins expression in KYSE-150 cells treated with LNT-SeNPs group (LNT-SeNPs) and LNT-SeNPs + Nab-PTX group (the Compound group). (**C**) Representative TEM images of KYSE-150 cells treated with LNT-SeNPs, Nab-PTX, or both (white arrows indicate normal ER, red arrows indicate swollen ER, yellow arrows indicate autophagosomes, and the MIT indicates mitochondria). (**D**) Schematic illustration on the enhancement of SelN-mediated ER stress by LNT-SeNPs. (**E**) The expression of IRE1α, IRE1α (S724), CHOP, and Bcl2 in KYSE-150 cells and KYSE-150/shSelN cells treated with 64 ng/mL Nab-PTX and 8 μM LNT-SeNPs after 48 h. Cell viability of (**F**) KYSE-150 cells, and (**G**) KYSE-150/shSelN cells treated with 64 ng/mL Nab-PTX and 8 μM LNT-SeNPs after 48 h. Calcium level in the ER of (**H**) KYSE-150 cells, and (**I**) KYSE-150/shSelN cells treated with 64 ng/mL Nab-PTX and 8 μM LNT-SeNPs after 48 h. All data are shown as mean ± SD ($n = 3$). *$P < 0.05$, **$P < 0.01$, ***$P < 0.001$, ****$P < 0.0001$

down to establish the KYSE-150/shSelN cell line for further verification. Western blotting analysis on the ER stress-related signaling pathways (IRE1α-CHOP-Bcl2 axis) was thus further evaluated in both normal KYSE-150 cells and knockdown KYSE-150/shSelN cells. As shown in Fig. 4E, the relative expression of IRE1α (S724) (1.8), and CHOP (3.1) and Bcl2 (0.3) in normal KYSE-150 cells was significantly elevated by the co-stimulation of LNT-SeNPs and Nab-PTX. Correspondingly, the relative expression of Bcl2 (0.6) was distinctively decreased. In contrast, owing to the knockdown of SelN, the relative expression of IRE1α (S724) (1.1), and CHOP (1.4), and Bcl2 (0.6) in KYSE-150/shSelN cells from Compound group was comparable to that from Nab-PTX group (1.08, 1.38, 0.61), indicating the essential role of SelN in mediating the IRE1α-CHOP-Bcl2 axis to promote ER stress in KYSE-150 cells. The combinative antitumor effect of LNT-SeNPs and Nab-PTX was further verified on both normal KYSE-150 cells and SelN knockdown KYSE-150/shSelN cells. As shown in Fig. 4F and G and Figure S4, under the treatment of Nab-PTX, LNT-SeNPs or both, the difference on cell viability of normal KYSE-150 cells from each treatment group was distinct. While in SelN knockdown KYSE-150/shSelN cells, the cell viability between the Nab-PTX group and Compound group was comparable without obvious difference, preliminarily demonstrating the very indispensable role of SelN in mediating the ER stress in KYSE-150 cells. The same (Fig. 4H and I), the calcium level in ER of KYSE-150/shSelN cells also exhibited the similar trend as the fluorescence intensity of BBcellprobe C93 from Nab-PTX group and Compound group was nearly the same. It's noteworthy that the fluorescence intensity of BBcellprobe C93 in the LNT-SeNPs group was elevated, even though the cell viability remained high in normal KYSE-150 cells, demonstrating the essential role of LNT-SeNPs in promoting ER stress.

Taken together, considering the very indispensable role of LNT-SeNPs in mediating ER stress-related signaling pathways to synergize the antitumor efficacy of Nab-PTX, it could be deduced that the supplementation of LNT-SeNPs during the conventional Nab-PTX therapy in ESCC may be highly feasible in clinic.

In vivo synergistic antitumor efficacy of LNT-SeNPs and Nab-PTX on KYSE-150 tumor-bearing model

The synergistic antitumor efficacy of LNT-SeNPs and Nab-PTX was thus investigated on BALB/c nude bearing KYSE-150 xenografts as depicted in Fig. 5A. Before the therapeutic evaluation, the global biodistribution of LNT-SeNPs through i.v. administration was studied in advance. As detected in Fig. 5B, after single dosage of ICG-SH-loaded LNT-SeNPs, strong fluorescence intensity could be detected at 24 h-post injection in tumor tissues and the nanoparticles could retained for another 48 h. Therefore, the administration frequency of LNT-SeNPs was fixed to every 3 days in the following therapeutic evaluation.

After 28 days in vivo therapeutic evaluation, it is astonishing to be seen in Fig. 5C that, G4 group (0.5 mg/kg LNT-SeNPs and 20 mg/kg Nab-PTX) with the half dosage of G5 group (40 mg/kg Nab-PTX) exhibited the similar inhibition effect on the tumor growth. In contrast, the resected tumor from G3 group (20 mg/kg Nab-PTX) was larger than that of G4 or G5 group. Besides that, the resected tumor from G2 group was comparable to G1 group, preliminarily suggesting the low dosage (0.5 mg/kg) of LNT-SeNPs was safe to the tissues including the tumor tissues. Moreover, the great synergistic antitumor effect was applicable in both male and female mice models. The growth curve of tumor volume from each treatment group more distinctively demonstrated the synergistic antitumor efficacy between LNT-SeNPs and Nab-PTX. As indicated in Fig. 5D and E, tumor volume from both G4 and G5 group was contained around 200 mm3 while in G3 group, the tumor volume was hardly to be contained in the later stage and climbed to around 500 mm^3, highlighting the very antitumor efficacy of LNT-SeNPs and Nab-PTX on ESCC. Meanwhile, the body weight change during the evaluation (Fig. 5F and G) also demonstrated the co-treatment of LNT-SeNPs and Nab-PTX was a wide-applicable, efficient and highly safe therapeutic strategy as both male and female mice weights from G4 group were steady during the whole evaluation and the trend was similar to the G1 group.

Therefore, the synergistic antitumor efficacy of LNT-SeNPs and Nab-PTX was further investigated by histological analysis. As observed in Fig. 5H, compare with G1 group, pathological changes were hardly to detect in the liver and kidney slices from G4 group, underlying the

biosafety of the co-treatment of LNT-SeNPs and Nab-PTX. While in the tumor slices, in comparison with the highly active division in G1 group, the purple color representing the status of nucleus was significantly decreased in tumor tissues from G4 group. The proliferation status of tumor was further analyzed by immunohistochemistry. As shown in Fig. 5I, the apoptosis (presented as brownish area) was significantly elevated in tumor tissues from G4 group. This phenomenon was also detected in tumor tissues from the other treatment groups in different extents, which was consistent the results of tumor volume growth curve. Correspondingly, Ki67 expression, representing the proliferation of cancer cells, was greatly decreased in tumor tissues from G4 group. All these data demonstrated that the co-treatment of LNT-SeNPs and Nab-PTX was efficient and highly safe strategy to treat ESCC.

Therefore, the biosafety of such treatment strategy was further investigated by serum biochemical analysis. As indicated in Fig. 5J and M and S7, the administration of Nab-PTX distinctively disturbed the liver and kidney function, especially in high dosage (40 mg/kg), as the index levels of ALT, AST, TG, TC, creatinine, and urea were increased severalfold in comparison with the control group. In contrast, all these indices level from G4 group, though elevated slightly, were all contained in normal range, confirming the satisfactory biosafety of the co-treatment of LNT-SeNPs and Nab-PTX. In order to confirm the satisfactory biosafety was derived from the function of selenium, we preliminarily determined the selenium concentration both in mice serum and tumor tissues. As shown in Fig. 5N and O, selenium concentration in G4 group was much higher than that form G3 and G5 group, which was comparable with the selenium concentration in G2 group.

Overall, it could be concluded the supplementation of LNT-SeNPs with low dosage during the ESCC treatment by Nab-PTX may synergistic the antitumor efficacy and significantly mitigate the adverse effects or toxicity resulting from a high dose of Nab-PTX. which may be translated as a wide-applicable, efficient and highly safe therapeutic strategy for clinical treatment of ESCC.

Immune response induced by LNT-SeNPs and Nab-PTX through SelN-mediated ER stress

Considering the highly metastasis potential of ESCC in later stage, the immune status of mice was also evaluated by Elisa kits to determine the cytokine levels in mice serum and tumor tissues. As indicated in Fig. 6A and D, the levels of TNF-α (representing the innate immune response) and IFN-γ (representing the adaptive immune response) in serum or tumor tissues from both male and female mice models co-treated with LNT-SeNPs and Nab-PTX were significantly enhanced. Intriguingly, though exhibiting the similar antitumor efficacy, 40 mg/kg Nab-PTX did not distinctively promote the mice immune response, considering its side-effects and toxicity to the major organs. Therefore, all these data proved, except for the great synergistic antitumor efficacy through promoting cell apoptosis, the co-treatment of LNT-SeNPs and Nab-PTX may also efficiently trigger the specific antitumor immune response to fight against ESCC.

Therefore, the essential role of SelN in mediating this entire antitumor activity was further verified in tumor tissues. As detected in Fig. 6E and F, strong Ca^{2+} signal presenting as green fluorescence was only observed in G2 and G4 group with LNT-SeNPs administration. Correspondingly, apparent up-regulation on SelN expression was also observed in G2 and G4 group. Concluding from all these results, it could be deduced that through the supplementation of LNT-SeNPs, mice underwent Nab-PTX therapy may better trigger the specific antitumor immune response through the autophagy induced by the SelN-mediated ER stress in tumor tissues, which is observed in the aforementioned TEM results for KYSE-150 cells.

Conclusions

In this essay, we screened the inhibitory effect of selenium-containing drugs ($SeCys_2$, SeM, Na_2SeO_3, and LNT-SeNPs) on ESCC cell line (KYSE-150 cells) and revealed the underlying synergistic potential of LNT-SeNPs on promoting the antitumor efficacy of Nab-PTX. Investigation on KYSE-150 cells demonstrated that Nab-PTX in combination with a low dosage (8 μM) of LNT-SeNPs may synergistically improve its antitumor efficacy on ESCC cells through promoting the apoptosis and inhibiting the metastasis. Proteomics analysis revealed the core mechanism of LNT-SeNPs on promoting the antitumor efficacy of Nab-PTX was significantly relied on the excessive Ca^{2+} accumulation in ER induced by SelN-mediated ER stress-related signaling pathways. SelN knockdown KYSE-150 cell model (KYSE-150/shSelN cells) further confirmed the very indispensable role of SelN in mediating the synergistic effect on promoting the antitumor efficacy of Nab-PTX. Moreover, in vivo evaluation on KYSE-150 tumor-bearing mice models also demonstrated the supplementation of LNT-SeNPs with low dosage (0.5 mg/kg, i.v.) during the ESCC treatment by Nab-PTX may synergize the antitumor efficacy and significantly mitigate the adverse effects or harmfulness resulting from elevated doses of Nab-PTX. Overall, along with the facile accessibility of raw materials, this study reports LNT-SeNPs as a synergistic agent to promote the antitumor efficacy of Nab-PTX, which may be translated as a wide-applicable, efficient and highly safe strategy for clinical treatment of ESCC.

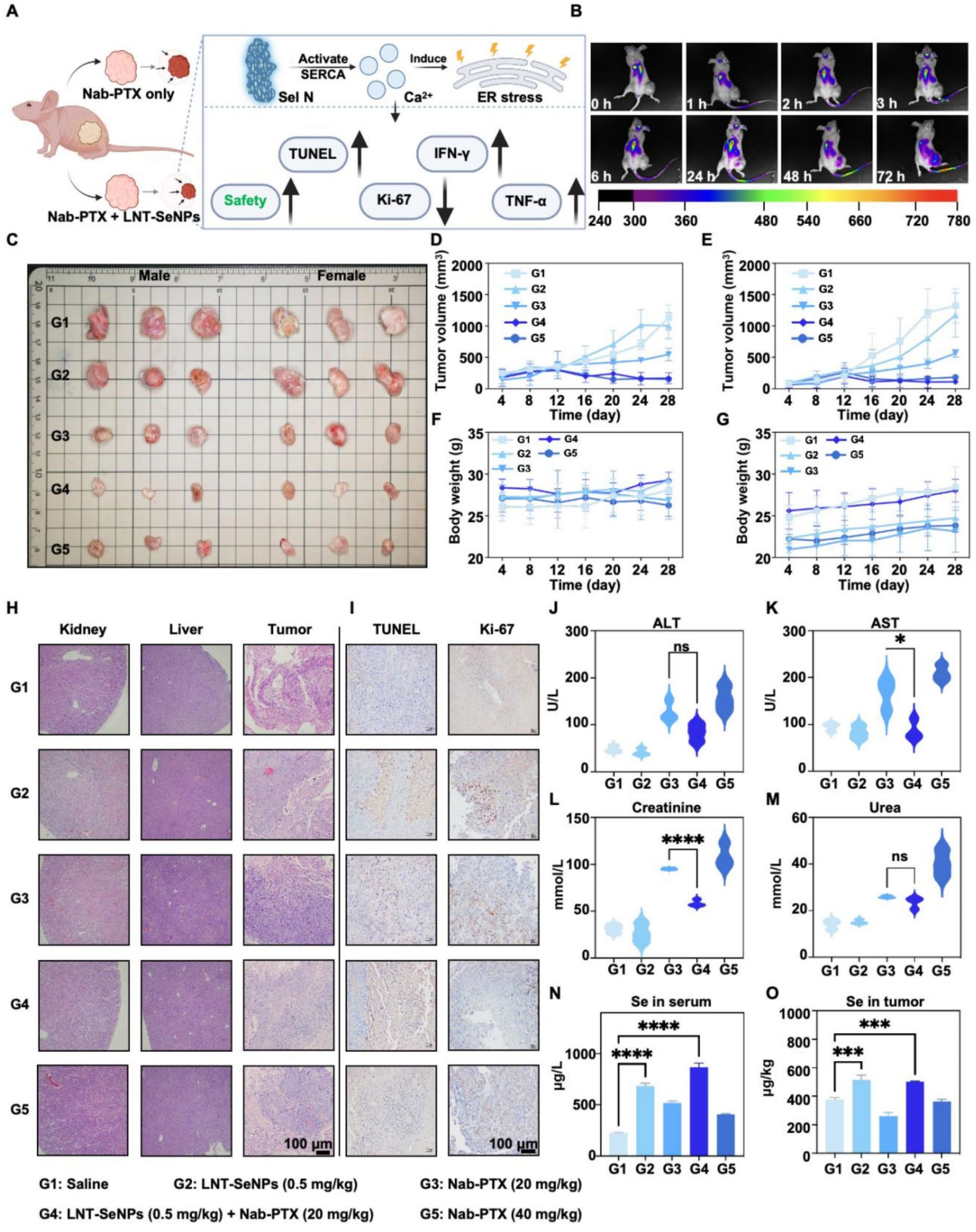

Fig. 5 (See legend on next page.)

(See figure on previous page.)

Fig. 5 In vivo synergistic antitumor efficacy of LNT-SeNPs and Nab-PTX on BALB/c nude bearing KYSE-150 xenografts. (**A**) Schematic diagram of the evaluation protocol for BALB/c nude bearing KYSE-150 xenografts, assigned to five groups: G1 (saline, i.v.), G2 (0.5 mg/kg LNT-SeNPs, i.v.), G3 (20 mg/kg Nab-PTX, i.v.), G4 (0.5 mg/kg LNT-SeNPs and 20 mg/kg Nab-PTX, i.v.), and G5 (40 mg/kg Nab-PTX, i.v.). (**B**) Global biodistribution profile of BALB/c nude bearing KYSE-150 xenografts administered with ICG-SH-loaded LNT-SeNPs in 72 h. (**C**) Photos depicting excised tumors from various therapeutic cohorts. The plot of tumor volume vs. time from (**D**) male, and (**E**) female mice in each treatment group. Body weight changes in (**F**) male, and (**G**) female mice during the whole evaluation. (**H**) Histological analysis of kidney, liver, hematoxylin and eosin staining highlighted the tumor sections, with a scale indicator = 50 μm. (**I**) Immunohistochemical analysis of TUNEL and Ki-67 expression in slices of tumor, scale indicator = 50 μm. Serum biochemical analysis of liver and kidney function including (**J**) alanine aminotransferase (ALT), (**K**) aspartate aminotransferase (AST), (**L**) creatinine, (**M**) urea level in each treatment group. Se concentrations in mice (**N**) serum and (**O**) tumor tissues determined by ICP. All data are shown as mean ± SD ($n = 3$). *$P < 0.05$, **$P < 0.01$, ***$P < 0.001$, ****$P < 0.0001$

Materials and methods

Materials

For our experiment, we acquired $SeCys_2$, SeM, and Na_2SeO_3 from Aladdin based in Shanghai. Lentinan and ascorbic acid were also sourced from this supplier. We procured PI, ER tracker, and Fluo-4-AM, which are essential fluorescent probes, from Thermo Fisher Scientific in the United States. For the immunological aspect, Cell Signaling Technology provided us with antibodies targeting PERK, CHOP, and Bcl2. Additionally, we secured a specific anti-PERK antibody from Abcam in Cambridge, UK, and anti-SelN came from Santa Cruz Biotechnology. To measure cytokine levels, we used ELISA kits designed for IFN-γ, TGF-β, and TNF-α, which we obtained from Solarbio Co., Ltd in Beijing.

Synthesis and characterization of LNT-SeNPs

LNT-SeNPs were prepared according to our previously reported protocol. In brief, 2 mL LNT solution at a concentration of 1 mg/mL was firstly prepared and extruded through 0.22 μm filter membrane for further use. 2 mL, 10 mM Na_2SeO_3 solution was then mixed with the above solution at volume ratio of 1:1 (V/V). After that, 2 mL, 40 mM Vc solution was added into the above mixture drop wisely with the volume constant to 10 mL. After reaction for 10 h, the resultants (LNT-SeNPs) were dialyzed against ultrapure water for 24 h to remove the unreacted LNT, Na_2SeO_3 and Vc. The morphology, size distribution, surface charge, and chemical structure of LNT-SeNPs were investigated by transmission electron microscope (TEM, Hitachi H-7650, 100 kV), Malvern zetasizer (Malvern Instruments Co., Ltd., UK), and X-ray photoelectron spectroscopy (XPS, Thermoescalab 250Xi). The selenium content in LNT-SeNPs was quantified using ICP-MS.

Cell line and cell culture

We acquired KYSE-150 cells, a type of esophageal squamous carcinoma line, from the American Type Culture Collection in Manassas, Virginia. Another variant, KYSE-150/shSelN, was obtained from Haixing Biosciences in Suzhou, China. We cultured these cells in 1640 Medium, enriched with penicillin (100 units per milliliter) and streptomycin (50 units per milliliter), along with a 10% addition of fetal bovine serum. The incubation took place at 37 degrees Celsius within a moist environment, supplemented by 5% carbon dioxide.

Cytotoxicity of LNT-SeNPs on KYSE-150 cells

To assess the cytotoxicity, the KYSE-150 cells were used to investigate the antitumor efficacy of LNT-SeNPs on ESCC through CCK-8 assay. Briefly, we plated KYSE-150 cells at a density of 2,000 cells per well into a 96-well plate, followed by an overnight incubation. After that, cells were treated with various selenium-containing drugs ($SeCys_2$, SeM, Na_2SeO_3, LNT-SeNPs, 0–32 μM), Nab-PTX (0-128 ng/mL), or the mixture of Nab-PTX (0-128 ng/mL) and LNT-SeNPs (1–8 μM). Incubate for 48 h, then introduce CCK-8 to each well and allow for an additional 2-hour incubation period. Finally, detect 96-well plate with microplate reader (Gene 5, Biotek) at 450 nm, and the cell viability of each treatment group was calculated by percentage to the control group. The synergistic antitumor efficacy between LNT-SeNPs and Nab-PTX was analyzed by SynergyFinder website.

EdU assay

The synergistic antitumor efficacy between LNT-SeNPs and Nab-PTX was further investigated by EdU assay. In brief, we plated KYSE-150 cells at a density of 20,000 cells per well into a 6-well plate and allowed them to incubate overnight. After that, we add 8 μM LNT-SeNPs, 64 ng/mL Nab-PTX, or both of them in to the plate. Cells underwent a wash with PBS following a 24-hour incubation, then received a 2-hour treatment with EdU. Finally, the proliferation status of each treatment group was detected under fluorescent microscope according to the protocol provided by manufacturer.

Cell cycle arrest induced by LNT-SeNPs and Nab-PTX

We utilized flow cytometry to assess the combination impact of LNT-SeNPs and Nab-PTX on the cellular cycle. In brief, KYSE-150 cells with a density of 20,000 cells/well were seeded into 6-well plate and incubated overnight. After that, cells were treated with 8 μM LNT-SeNPs, 64 ng/mL Nab-PTX, or both. After incubation, cells were collected and fixed with 75% ethanol at -20 °C for 4 h. After incubation, cells were centrifuged and stained with PI for 30 min. Cell cycle profile from each

treatment group was finally analyzed by flow cytometry (Cytoflex, Beckman) and quantified by FlowJo software.

Apoptosis induced by LNT-SeNPs and Nab-PTX

The apoptosis induced by LNT-SeNPs and Nab-PTX was also studied by flow cytometry. Likewise, KYSE-150 cells received an 8 μM dose of LNT-SeNPs, a 64 ng/mL Nab-PTX treatment, or both. Subsequently, the cells underwent staining using Annexin V-FITC and propidium iodide, in preparation for subsequent flow cytometric analysis. (Cytoflex, Beckman).

Colony formation assay

We employed crystal violet staining to evaluate the synergistic impact of LNT-SeNPs with Nab-PTX on KYSE-150 cell growth. KYSE-150 cells were plated at 1000 cells per well in a 6-well plate and allowed to incubate overnight. After that, cultured cells underwent treatment with either 4–8 μM LNT-SeNPs, 64 ng/mL Nab-PTX, or both, and were then incubated over a period of seven days, cells underwent fixation with methanol followed by staining using a crystal violet solution. Representative photos from each treatment group were finally capture under multifunctional detection system (Gene 5.0, Biotek).

In vitro invasion assay

Transwell was used to evaluate the combinative effect of LNT-SeNPs and Nab-PTX on cell invasion according to our previously reported protocol. In brief, upper chamber was seeded with KYSE-150 cells (2.5 × 105 cells/well) while bottom chamber was dispersed with 4–8 μM LNT-SeNPs, 64 ng/mL Nab-PTX, or both. After 24 h incubation, we fixed the cells using methanol and applied Giemsa stain before examining them under a Leica optical microscope (Leica, Germany). The invaded cells were quantified by Image J software.

Proteomics analysis

The expression of selenoproteins and ER stress-related proteins in KYSE-150 cells was analyzed using proteomics. Briefly, We plated KYSE-150 cells at a density of 20 million cells per well into 15 cm dishes and allowed them to settle overnight. After that, cells were treated with 8 μM LNT-SeNPs, 64 ng/mL Nab-PTX, or both. After that, protein samples were collected and the proteomics sequencing services were provided by Chi Biomedicine, Inc. (Shenzhen China).

ER stress induced by LNT-SeNPs and Nab-PTX

The ER stress in KYSE-150 cells induced by LNT-SeNPs and Nab-PTX was investigated by TEM (JEOL, Japan). Briefly, we seeded KYSE-150 cells with a density of 5×10^6 cells/well were into 6-well plate and incubated for about 24 h. After that, we treated cells with 8 μM LNT-SeNPs, 64 ng/mL Nab-PTX, or both. After incubation for 48 h, the cells underwent fixation by being immersed in a solution containing 2% paraformaldehyde and 0.2% glutaraldehyde within a sodium cacodylate buffer at a pH of 7.4. This process was carried out at a temperature of 37 degrees Celsius for a duration of one hour, and then dehydrated for the final detection of ER status under high-resolution transmission electron microscope (HRTEM, JEM-2100). In order to visualize the accumulation of Ca^{2+} in ER, Mag-Fluo-4 AM and ER-tracker from AAT bioquest were used. In brief, KYSE-150 cells were seeded in 24-well plate at 1×10^5 cells per well. After overnight incubation, cells were rinsed and stained with 5 μM Mag-Fluo-4 AM. After another 45 min incubation, cells were rinsed with 1 mM Probenecid (20062, AAT Bioquest) and incubated for 10 min. Cells were rinsed and stained with ER-tracker (22636, AAT Bioquest) and DAPI (17510, AAT Bioquest) for 30 min. After washed with medium, cells were incubated for another 20 min to complete de-esterification and finally captured with a confocal microscope (Zeiss, Germany) For the determination of Ca^{2+} in ER, KYSE-150 cells were firstly proceeded as the above protocols. After that, BBcellprobe®C93 was used to quantify the level of calcium ions in ER according to the protocol provided by the manufacturer.

In vivo antitumor efficacy of LNT-SeNPs

In our study, we developed BALB/c nude mice models with KYSE-150 xenografts to assess the collaborative anti-cancer potential of Nab-PTX when used in conjunction with LNT-SeNPs. In brief, BALB/c nude mice were subcutaneously injected with 1×10^6 KYSE-150 cells at first and randomly assigned into 5 groups once the tumor volume reached 150 mm3: G1 (100 μL saline, i.v.), G2 (0.5 mg/kg LNT-SeNPs, i.v.), G3 (20 mg/kg Nab-PTX, i.v.), G4 (0.5 mg/kg LNT-SeNPs and 20 mg/kg Nab-PTX, i.v.), and G5 (40 mg/kg Nab-PTX, i.v.). The whole evaluation lasted for 28 days, during which the data including body weight, tumor width and length were collected every 4 days. All drug formulations were i.v. administered every 3 days. At the endpoint, mice from each treatment group were all euthanized and the major organs including liver, kidney, tumor, and serum were collected for further investigation. Se concentration in tumor tissues and serum were determined by Inductively coupled plasma mass spectrometry (ICP-MS). Serum levels of alanine aminotransferase (ALT), aspartate aminotransferase (AST), creatinine, urea, triglycerides (TG), total Cholesterol (TC), and albumin (ALB) were determined by an automatic biochemical analyzer. Cytokine levels including IFN-γ, TGF-β, and TNF-α in tumor tissues and serum were determined by corresponding Elisa kits according to the manufacturer's protocols.

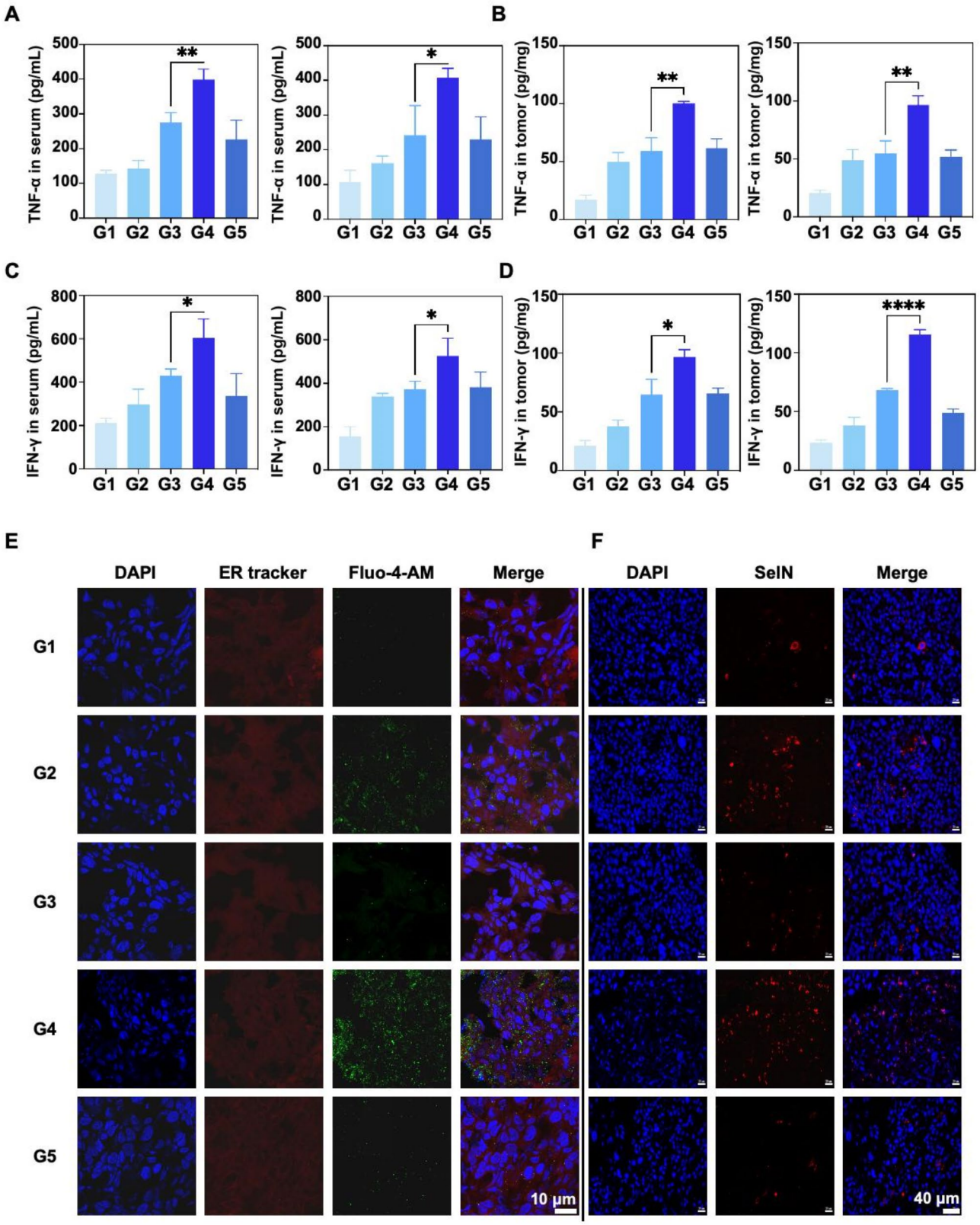

Fig. 6 LNT-SeNPs promote cytokine secretion and Nab-PTX -induced ER stress. TNF-α levels in mice serum and tumor tissues from (**A**) male, and (**B**) female mice in each treatment group. IFN-γ levels in mice serum and tumor tissues from (**C**) male, and (**D**) female mice in each treatment group. (**E**) Representative fluorescent images of ER tracker and Fluo-4-AM co-stained tumor tissues from each treatment group. (**F**) Representative fluorescent images of SelN-stained tumor tissues from each treatment group. All data are shown as mean ± SD ($n = 3$). *$P < 0.05$, **$P < 0.01$, ***$P < 0.001$, ****$P < 0.0001$

Biodistribution of LNT-SeNPs

BALB/c nude mice bearing KYSE-150 xenografts was used to investigate the global biodistribution of LNT-SeNPs. Briefly, BALB/c nude mice bearing KYSE-150 xenografts were intravenously injected with 0.5 mg/kg ICG-SH-loaded LNT-SeNPs and the fluorescent photos were then capture at specific time intervals (0, 1, 2, 3, 6, 24, 48, 72 h-post injection) by IVIS Spectrum (Perkin Elmer, USA).

Western blotting analysis

Collected cell samples were homogenized in RIPA buffer, lysed for 30 min and then centrifuged at 12,000 rpm for 15 min to obtain the supernatant for further electrophoresis. Protein concentration of each sample was determined by BCA kit. After that, the expression of target proteins (SelN, IRE1α, IRE1α(S724), CHOP and Bcl2) was analyzed by western blotting according to our previously reported protocol. GAPDH was used as an internal reference to confirm the same loading in each lane. Protein expression was analyzed and quantified by the ImageJ software.

Histological analysis

H&E staining, immunofluorescent, immunohistochemical analysis of tumor, liver, and kidney slices were used to investigate the pathological status in tissues. In brief, collected organs were fixed in 4% paraformaldehyde to dehydrate and then sliced. After that, slices were dewaxed, rehydrated, and then stained with hematoxylin and eosin according to the protocol. The pathological status in tissues was then detected under Vectra Automated Quantitative Pathology Imaging System (PerkinElmer).

Immunohistochemical analysis

Tumor slices were dewaxed and rehydrated followed with 45 s microwave oven heating to retrieve antigen. After that, slices were mounted with 3% H_2O_2 and then blocked with 10% goat serum for 1 h. After washing with PBST for 3 times, slices were mounted with primary antibodies and incubated at 4 °C overnight. After the incubation, tumor slices were mounted with HRP-conjugated antibody for another 1 h and then stained with DAB substrate for further detection *via* Vectra Automated Quantitative Pathology Imaging System (PerkinElmer, USA).

Immunofluorescent analysis

Tumor slices were proceeded similar to the protocol of immunohistochemical analysis with primary antibodies replaced by fluorescence-labeled primary antibodies.

Statistical analysis

We presented values as the average with a standard deviation. We assessed differences between groups through one-way ANOVA or the Student's t-test with GraphPad Prism version 5.0 for Windows. We regarded p-values < 0.05, 0.01, 0.001, or 0.0001 as noteworthy indicators of statistical significance.

Supplementary Information

The online version contains supplementary material available at https://doi.org/10.1186/s12951-025-03356-4.

Supplementary Material 1

Acknowledgements

We highly appreciate the efforts bringing from the College of Chemistry and Materials Science lab, Jinan University. Parts of the diagram, Figs. 4 and 5 were drawn by using templates from Biorender.

Author contributions

H.H. and L.X. conceived and planned this project; H.H. performed the key experiments; H.H., S.L. and H.L. edited the manuscript; S.L. and Z.W. assisted in the experiments; H.H. and S.L. contributed to data interpretation and manuscript preparation; H.H. drafted the manuscript with feedback and revisions from all authors. T.C., J.W., and J.L. supervised the study, reviewed and revised the manuscript. All authors examined and endorsed the final manuscript.

Funding

This work was supported by the Guangzhou Science, Technology Planning Project (2060206), National Key Research and Development Program of the Ministry of Science and Technology of China (2022YFB4702604), National Natural Science Foundation of China (32171296), The National Natural Science Foundation for Distinguished Young Scholars (82225025), National Key R&D Program of China (2023YFC3402800), and Open project Fund of Guangdong Key Laboratory of Functional Coordination Supramolecular Materials and Applications (2022A02).

Data availability

No datasets were generated or analysed during the current study.

Declarations

Ethical approval and consent to participate

This study was approved by the Animal Care and Use of Affiliated First Hospital of Guangzhou Medical University (20240356). All animal procedures were performed under national and institutional ethic guidelines for the care and use of laboratory animals.

Consent for publication

Not applicable.

Competing interests

The authors declare no competing interests.

Author details

[1]Department of Thoracic Surgery and Oncology, State Key Laboratory of Respiratory Disease & National Clinical Research Center for Respiratory Disease, The First Affiliated Hospital of Guangzhou Medical University, Guangzhou 510120, China
[2]Pulmonary and Critical Care Medicine, Guangzhou Institute of Respiratory Health, National Clinical Research Center for Respiratory Disease, National Center for Respiratory Medicine, State Key Laboratory of Respiratory Diseases, The First Affiliated Hospital of Guangzhou Medical University, Guangzhou 510120, China
[3]Department of Chemistry, Jinan University, Guangzhou 510632, China

Received: 27 December 2024 / Accepted: 24 March 2025
Published online: 15 April 2025

References

1. Jeon WJ, Park D, Al-Manaseer F, Chen Y-J, Kim JY, Liu B, et al. Survival and treatment patterns in stage II to III esophageal cancer. JAMA Netw Open. 2024;7:e2440568.
2. Lu Z, Chen Y, Liu D, Jiao X, Liu C, Wang Y, et al. The landscape of cancer research and cancer care in China. Nat Med. 2023;29:3022–32.
3. Liu X, Zhao S, Wang K, Zhou L, Jiang M, Gao Y, et al. Spatial transcriptomics analysis of esophageal squamous precancerous lesions and their progression to esophageal cancer. Nat Commun. 2023;14:4779.
4. Kumagai S, Koyama S, Shitara K. Precise patient stratification in esophageal cancer: biomarkers for immunochemotherapy. Cancer Cell. 2023;41:1199–201.
5. Wu L, Li B, Wan G, Wang Y, Zhu J, Liang L, et al. Toripalimab plus chemotherapy and radiotherapy for treatment-naive advanced esophageal squamous cell carcinoma: a single-arm phase 2 trial. Nat Commun. 2024;15:7116.
6. Wang Q, Yu Y, Wang C, Jiang Z, Li J, Li X, et al. Heterogeneity of tertiary lymphoid structures predicts the response to neoadjuvant therapy and immune microenvironment characteristics in triple-negative breast cancer. Br J Cancer. 2024;132:1–16.
7. Molinari C, Marisi G, Laliotis G, Spickard E, Rapposelli IG, Petracci E, et al. Assessment of Circulating tumor DNA in patients with locally advanced rectal cancer treated with neoadjuvant therapy. Sci Rep. 2024;14:29536.
8. Menzies AM, Amaria RN, Rozeman EA, Huang AC, Tetzlaff MT, van de Wiel BA, et al. Pathological response and survival with neoadjuvant therapy in melanoma: a pooled analysis from the international neoadjuvant melanoma consortium (INMC). Nat Med. 2021;27:301–9.
9. Nichetti F, Rota S, Ambrosini P, Pircher C, Gusmaroli E, Droz Dit Busset M, et al. NALIRIFOX, FOLFIRINOX, and gemcitabine with Nab-Paclitaxel as First-Line chemotherapy for metastatic pancreatic cancer: A systematic review and Meta-Analysis. JAMA Netw Open. 2024;7:e2350756.
10. Li Q, Liu J, Zhang Q, Ouyang Q, Zhang Y, Liu Q, et al. The anti-PD-L1/CTLA-4 bispecific antibody KN046 in combination with nab-paclitaxel in first-line treatment of metastatic triple-negative breast cancer: a multicenter phase II trial. Nat Commun. 2024;15:1015.
11. Catanzaro E, Beltrán-Visiedo M, Galluzzi L, Krysko DV. Immunogenicity of cell death and cancer immunotherapy with immune checkpoint inhibitors. Cell Mol Immunol. 2024;22:1–16.
12. Wang B, Sun T, Zhao Y, Wang S, Zhang J, Wang Z, et al. A randomized phase 3 trial of gemcitabine or Nab-paclitaxel combined with cisplatin as first-line treatment in patients with metastatic triple-negative breast cancer. Nat Commun. 2022;13:4025.
13. Klein-Brill A, Amar-Farkash S, Lawrence G, Collisson EA, Aran D. Comparison of FOLFIRINOX vs gemcitabine plus Nab-Paclitaxel as First-Line chemotherapy for metastatic pancreatic ductal adenocarcinoma. JAMA Netw Open. 2022;5:e2216199.
14. Zhang Y, Wang X, Niu X, Wang H, Wu Y, Li C, et al. Multi-therapeutic-activity selenium nanodot toward preventing brain injury and restoring neurobehavioral functions following hemorrhagic stroke. J Nanobiotechnol. 2024;22:564.
15. Huai M, Pei M, Chen J, Duan X, Zhu Y, Yang F, et al. Oral creatine-modified selenium-based hyaluronic acid nanogel mediated mitochondrial energy recovery to drive the treatment of inflammatory bowel disease. J Nanobiotechnol. 2024;22:740.
16. He W, Tian X, Zhou Q, Lv J, Li Y, Jin C, et al. Selenium nanoparticles ameliorate lumbar disc degeneration by restoring GPX1-mediated redox homeostasis and mitochondrial function of nucleus pulposus cells. J Nanobiotechnol. 2024;22:634.
17. Wang R, Ha K, Dhandapani S, Kim Y-J. Biologically synthesized black ginger-selenium nanoparticle induces apoptosis and autophagy of AGS gastric cancer cells by suppressing the PI3K/Akt/mTOR signaling pathway. J Nanobiotechnol. 2022;20:441.
18. El-Badri AM, Hashem AM, Batool M, Sherif A, Nishawy E, Ayaad M, et al. Comparative efficacy of bio-selenium nanoparticles and sodium selenite on morpho-physiochemical attributes under normal and salt stress conditions, besides selenium detoxification pathways in brassica Napus L. J Nanobiotechnol. 2022;20:163.
19. Lai H, Xu L, Liu C, Shi S, Jiang Y, Yu Y, et al. Universal selenium nanoadjuvant with Immunopotentiating and redox-shaping activities inducing high-quality immunity for SARS-CoV-2 vaccine. Signal Transduct Target Therapy. 2023;8:1–3.
20. Zou B, Xiong Z, He L, Chen T. Reversing breast cancer bone metastasis by metal organic framework-capped nanotherapeutics via suppressing osteoclastogenesis. Biomaterials. 2022;285:121549.
21. Zhang D, You Y, Xu Y, Cheng Q, Xiao Z, Chen T, et al. Facile synthesis of near-infrared responsive on-demand oxygen releasing nanoplatform for precise MRI-guided theranostics of hypoxia-induced tumor chemoresistance and metastasis in triple negative breast cancer. J Nanobiotechnol. 2022;20:104.
22. Chen Q, He L, Li X, Xu L, Chen T. Ruthenium complexes boost NK cell immunotherapy via sensitizing triple-negative breast cancer and shaping immunomicroenvironment. Biomaterials. 2022;281:121371.
23. Liu S, Wei W, Wang J, Chen T. Theranostic applications of selenium nanomedicines against lung cancer. J Nanobiotechnol. 2023;21:96.
24. Schoenmakers E, Marelli F, Jørgensen HF, Visser WE, Moran C, Groeneweg S, et al. Selenoprotein deficiency disorder predisposes to aortic aneurysm formation. Nat Commun. 2023;14:7994.
25. Zheng X, Toyama T, Siu S, Kaneko T, Sugiura H, Yamashita S, et al. Selenoprotein P expression in glioblastoma as a regulator of ferroptosis sensitivity: preservation of GPX4 via the cycling-selenium storage. Sci Rep. 2024;14:682.
26. Ren B, Situ J, Huang X, Tan Q, Xiao S, Li N, et al. Selenoprotein W modulates Tau homeostasis in an Alzheimer's disease mouse model. Commun Biology. 2024;7:1–16.
27. Vinceti M, Urbano T, Chiari A, Filippini T, Wise LA, Tondelli M, et al. Selenoprotein P concentrations and risk of progression from mild cognitive impairment to dementia. Sci Rep. 2023;13:8792.
28. Mita Y, Nakayama K, Inari S, Nishito Y, Yoshioka Y, Sakai N, et al. Selenoprotein P-neutralizing antibodies improve insulin secretion and glucose sensitivity in type 2 diabetes mouse models. Nat Commun. 2017;8:1658.
29. Kim H, Lee K, Kim JM, Kim MY, Kim J-R, Lee H-W, et al. Selenoprotein W ensures physiological bone remodeling by preventing hyperactivity of osteoclasts. Nat Commun. 2021;12:2258.
30. Ye X, Toyama T, Taguchi K, Arisawa K, Kaneko T, Tsutsumi R, et al. Sulforaphane decreases serum Selenoprotein P levels through enhancement of lysosomal degradation independent of Nrf2. Commun Biology. 2023;6:1–9.
31. Schwarz M, Meyer CE, Löser A, Lossow K, Hackler J, Ott C, et al. Excessive copper impairs intrahepatocyte trafficking and secretion of Selenoprotein P. Nat Commun. 2023;14:3479.
32. Chernorudskiy A, Varone E, Colombo SF, Fumagalli S, Cagnotto A, Cattaneo A, et al. Selenoprotein N is an Endoplasmic reticulum calcium sensor that links luminal calcium levels to a redox activity. Proc Natl Acad Sci. 2020;117:21288–98.
33. Lopez RE, Knable AL, Burruss JB. Ingestion of a dietary supplement resulting in selenium toxicity. J Am Acad Dermatol. 2010;63:168–9.
34. Liu J, Li W, Lin Y, Peng Y, Zhan M, Lai H, et al. Tumor microenvironment-responsive metal nanotherapeutics for breast cancer chemo-/immunotherapy. NPG Asia Mater. 2023;15:26.
35. Liu C, Lin R, Lai H, Pi F, Xue Q, Chen T, et al. Thermosensitive selenium hydrogel boosts antitumor immune response for hepatocellular carcinoma chemoradiotherapy. Nano Today. 2023;50:101823.
36. Bray F, Laversanne M, Sung H, Ferlay J, Siegel RL, Soerjomataram I, et al. Global cancer statistics 2022: GLOBOCAN estimates of incidence and mortality worldwide for 36 cancers in 185 countries. Cancer J Clin. 2022;74:229–63.
37. Liu S, Li N, Lai H, Xu L, Zeng Y, Chen X, et al. Selenium nanoparticles enhance NK Cell-Mediated tumoricidal activity in malignant pleural effusion via the TrxR1-IL-18RAP-pSTAT3 pathway. Adv Funct Mater. 2024;34:2401264.
38. Yang M, Tang Z, Li X, Yu Y, He L, Chen T. Designing macrophage membrane-engineered ruthenium/selenium nanoparticles to block bone metastasis of breast cancer. Nano Res. 2024;17:7504–12.
39. Xu Y, Lai H, Pan S, Pan L, Liu T, Yang Z, et al. Selenium promotes Immunogenic radiotherapy against cervical cancer metastasis through evoking P53 activation. Biomaterials. 2024;305:122452.
40. Liu C, Wang W, Lai H, Chen Y, Li L, Li H, et al. Biosynthesis of fungus-based oral selenium microcarriers for radioprotection and immuno-homeostasis shaping against radiation-induced heart disease. Bioactive Mater. 2024;37:393–406.
41. Li Z, Pan S, Tian Y, Liu S, Wei W, Wang J, et al. Selenium nanoparticles enhance the chemotherapeutic efficacy of pemetrexed against non-small cell lung cancer. Chin Chem Lett. 2024;35:110018.
42. Li Y, Liu T, Zheng R, Lai J, Su J, Li J, et al. Translational selenium nanoparticles boost GPx1 activation to reverse HAdV-14 virus-induced oxidative damage. Bioactive Mater. 2024;38:276–91.

43. He L, Chen Q, Lu Q, Yang M, Xie B, Chen T, et al. Autophagy-Inducing MoO_{3-x} nanowires boost Photothermal-Triggered cancer immunotherapy. Angew Chem Int Ed. 2024;136:e202404822.
44. Chen M, Wang J, Cai F, Guo J, Qin X, Zhang H, et al. Chirality-driven strong thioredoxin reductase Inhibition. Biomaterials. 2024;311:122705.

Publisher's note